Dissection of Gαs and Hedgehog Signaling Cross-talk Reveals Therapeutic Opportunities to Target Hedgehog-Dependent Tumors

Sarah Krantz[1], Braden A. Bell[1], Katherine Lund[1], Natalia Salinas Parra[1], Yeap Ng[1,2], Natalia De Oliveira Rosa[3], Saikat Mukhopadhyay[4], Brad St. Croix[5], Kavita Y. Sarin[6], Roberto Weigert[1,2], Francesco Raimondi[3], and Ramiro Iglesias-Bartolome[1]

ABSTRACT

Basal cell carcinoma (BCC), the most common human cancer, is driven by hyperactivation of the Hedgehog pathway mediated by Smoothened (SMO) signaling and Glioma-Associated Oncogene Homolog (GLI) transcription. Gαs and protein kinase A (PKA) negatively regulate Hedgehog signaling, offering a potential alternative BCC development and treatment pathway. In this study, using histology alongside bulk and single-cell RNA sequencing, we found that mouse BCC–like tumors that originate from Gαs pathway inactivation are highly similar to those driven by canonical Hedgehog signaling induced by constitutive SMO activation. Both pathways led to the expansion of basal stem cells in the skin, with tumor cells clustering in two distinct populations with markers for touch dome and isthmus stem cell–like cells. Interestingly, mutations that reduce Gαs and PKA activity were present in human BCC. Tumors from Gαs pathway inactivation were independent of the canonical Hedgehog regulators SMO and GPR161, establishing them as SMO-independent oncogenic Hedgehog signaling models. Finally, activation of the Gαs-coupled adenosine 2B receptor with BAY60-6583 counteracted oncogenic SMO, reducing Hedgehog signaling and tumor growth. Together, these findings offer a potential therapeutic strategy for BCC.

Significance: Gαs/PKA pathway inactivation drives Hedgehog-dependent basal cell carcinoma and can be counteracted by activation of the Gαs-coupled adenosine 2B receptor to suppress tumor growth, providing a potential treatment for Hedgehog-driven tumors.

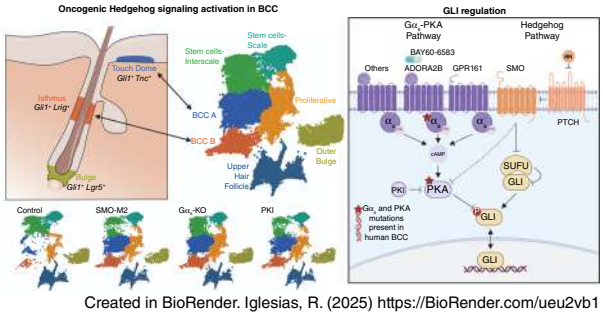

Created in BioRender. Iglesias, R. (2025) https://BioRender.com/ueu2vb1

Introduction

G protein–coupled receptors (GPCR) play a crucial role in regulating somatic stem cell activity, particularly in the skin, in which they control the balance of proliferation and differentiation and facilitate stem cell–niche interactions (1). The Frizzled class of GPCRs are central regulators of skin stem cell biology, including Smoothened (SMO), a key component of Hedgehog signaling. SMO is continuously repressed by patched receptors (PTCH) and is activated when secreted Hedgehog ligands bind to and inhibit PTCH (2). Active SMO blocks SUFU negative regulator of hedgehog signaling (SUFU), stabilizing the transcription factor Glioma-Associated Oncogene Homolog (GLI), which enters the nucleus and activates target gene transcription.

Hedgehog signaling is involved in numerous pathologies and is a primary driver of skin basal cell carcinoma (BCC). Mutations in PTCH and SMO are common in BCC, and overexpression of Hedgehog ligands and activated forms of SMO or GLI can cause BCC in mouse skin (3). BCC is the most frequent human cancer, with more than 3 million cases annually in the United States (4, 5). Most BCCs are easily treated by surgical removal, but a proportion of them can be challenging to treat due to their high numbers, location, or tumor spread (6). Alternative therapies like SMO inhibitors and immunotherapy face limitations due to side effects and resistance, highlighting the need for novel treatment options targeting Hedgehog-driven tumors.

Although BCC is considered to be mainly driven by alterations in canonical Hedgehog signaling, research has found a Gαs protein–dependent pathway vital to skin stem cell fate and BCC-like tumor formation (7). Gαs is one of the primary mediators of GPCR-G protein signaling, leading to the production of the second messenger cyclic AMP (cAMP). In mice, conditional epidermal deletion of the gene encoding Gαs (*Gnas*) results in BCC-like lesions (7). The effect

[1]Laboratory of Cellular and Molecular Biology, Center for Cancer Research, National Cancer Institute, National Institutes of Health, Bethesda, Maryland. [2]Intravital Microscopy Core, Center for Cancer Research, National Cancer Institute, National Institutes of Health, Bethesda, Maryland. [3]Laboratorio di Biologia Bio@SNS, Scuola Normale Superiore, Pisa, Italy. [4]Department of Cell Biology, University of Texas Southwestern Medical Center, Dallas, Texas. [5]Tumor Angiogenesis Unit, Mouse Cancer Genetics Program, National Cancer Institute, National Institutes of Health, Frederick, Maryland. [6]Department of Dermatology, Stanford University School of Medicine, Stanford, California.

Corresponding Author: Ramiro Iglesias-Bartolome, LCMB/CCR, National Cancer Institute, 37 Convent Drive, Building 37 Room 2050C, Bethesda, MD 20892. E-mail: ramiro.iglesias-bartolome@nih.gov

Cancer Res 2026;86:940–53

doi: 10.1158/0008-5472.CAN-25-1109

of Gαs on tumor formation is mediated by the cAMP-regulated protein kinase A (PKA). Blocking PKA also results in BCC-like tumors (7). Mechanistically, Gαs and PKA inhibition drive the activation of Hedgehog GLI and Hippo YAP1 (7), central mediators of tumor development. Although the negative regulation of Hedgehog signaling by PKA has been established over time (2), this research demonstrated that Gαs or PKA inactivation is sufficient to induce BCC-like tumor formation.

The precise mechanisms that link Gαs or PKA inactivation to oncogenic Hedgehog signaling remain unclear, representing a critical gap in our understanding of BCC pathogenesis. Deciphering this relationship is essential not only to identify novel therapeutic targets for Hedgehog-driven tumors but also to expand our knowledge of GPCR–Gαs interactions in stem cell and cancer biology. Here, we present a comprehensive analysis of BCC-like lesions driven by canonical oncogenic Hedgehog signaling and those caused by Gαs or PKA inactivation. Histological, bulk, and single-cell analyses reveal that BCC-like tumors from Gαs pathway inactivation are nearly indistinguishable from those arising from the canonical oncogenic Hedgehog pathway. Additionally, we demonstrate that mutations reducing Gαs and PKA activity are present in human BCC. Analysis of GPCR networks reveals that tumors arising from Gαs pathway inactivation are independent of the canonical Hedgehog regulators SMO and GPR161. Finally, we demonstrate that activation of the Gαs-coupled GPCR adenosine 2B receptor (ADORA2B) reduces tumor formation in a BCC mouse model. Our findings emphasize both the potential and limitations of activating GPCR–Gαs signaling as a therapeutic strategy for Hedgehog-driven tumors.

Materials and Methods

Mice

Mouse studies were approved by the Institutional Animal Care and Use Committee (IACUC) of the NCI, NIH. Lines from The Jackson Laboratory included LSL-SmoM2 (RRID:IMSR_JAX:005130), LSL-rtTA (RRID:IMSR_JAX:005670), K14CreERTM (RRID:IMSR_JAX:005107), *GliLz* reporter mice (RRID:IMSR_JAX:008211), K14Cre (RRID:IMSR_JAX:018964), and *Smo*-floxed mice (RRID:IMSR_JAX:004526). *Gnas*-floxed (8), *Gpr161*-floxed (9), and *Gpr124*-floxed mice (10) have been described before. TetO-PKA Inhibitor Protein (PKI) transgenic mice were generated by the CCR Transgenics Facility, as described previously (11), with a codon-optimized sequence for the 1 to 24 amino acids from human cAMP-dependent protein kinase inhibitor alpha (PKIA) downstream of GFP. Experiments used littermate controls, and both sexes were included. Knockouts in *Gpr124* and *Gpr161*-floxed mice were detected via PCR from tail DNA (primers in Supplementary Table S1). CreERTM was activated via tamoxifen injection (100 mg/kg; Sigma T5648) at 8 to 12 weeks. PKI expression was induced using doxycycline food (6 g/kg, Bio-Serv) after tamoxifen. Mice were randomized to receive drug treatments after tumor induction. Rolipram (Cayman Chemical, 10011132) and BRL50481 (Cayman Chemical, 16899) were injected intraperitoneally at 10 mg/kg/day, individually for 29 days starting 8 days after tamoxifen, or combined for 8 days, starting 40 days after tamoxifen. For topical drug treatments, isoproterenol (Sigma, I5627), 0.25 mg/site/day, and BAY 60-6583 (Tocris 4472), 10 μg/site/day, in DMSO were applied to the ear of mice for 10 days, starting 20 days after tamoxifen. Vismodegib (Selleckchem, S1082) was reconstituted in DMSO and diluted in 40% PEG-400 (Sigma, 91893) and 5% Tween-80 (Sigma, P8074) and injected intraperitoneally at 100 mg/kg/day for 10 days, 20 days after induction. In all cases, control mice received vehicle.

DNA constructs

Genes were cloned into a pCEFL vector using gene blocks (Integrated DNA Technologies). The GPR161-V129E mutation was introduced using the QuikChange II kit (Agilent). GPR161 constructs were cloned into pInducer20 (RRID:Addgene_44012). The *GNAS* sequence was based on the Gs long EE-tag (cDNA Resource Center, GNA0SLEI00). *PRKACA* was based on NM_002730.4 with a C-terminal HA tag. The SV40 LargeT lentivirus vector was from Addgene (RRID:Addgene_170255). The CRE reporter (pGL4.29-luc2P/CRE/Hygro) was from Promega. The GLI reporter (8xGLIBs) was constructed by cloning the 8x-Gli binding site from ref. 12 into pGL4.R-TRE-minPro (RRID:Addgene_211517). Human *GLI1* (NM_001160045.2) was cloned with a C-terminal HA and 3xGS linker into pLV-mCherry:T2A:Bsd-EF1A (VectorBuilder). The TEAD reporter (pGL3b-8xGTIIC-luciferase) was from Addgene (RRID:Addgene_34615).

Cell culture and transfections

Cells were cultured at 37°C with 5% CO_2. Lenti-X 293T cells for lentiviral production were from Takara Bio (632180, RRID:CVCL_4401). HEK293 cells were from AddexBio (cat. #T0011001/76, RRID:CVCL_0045). These cells were cultured in DMEM (Sigma, D5796) with 10% FBS (Sigma, F4135) and antibiotic/antimycotic solution (Sigma, A5955). N/TERT2G keratinocytes (11) were cultured in EpiLife media (Gibco, MEPI500CA) with Human Keratinocyte Growth Supplement (HKGS; Gibco, S0015). Transfections used Lipofectamine 3000 (Invitrogen). The SmoM2 BCC cell line and control mouse keratinocytes were isolated from the tail skin of SmoM2 mice or a control mouse [wild type (WT)] as described previously (13). Cells were plated on Culturex BME2 (3533-005-02) in EpiLife + HKGS + 10 μmol/L Y-27632 (Cayman Chemical, 10005583) + 10 ng/mL EGF (PeproTech, 315-09) and immortalized using SV40 large T. Control mouse keratinocytes were kept at this stage in the same culture conditions. SmoM2 were switched to DMEM + 10% FBS + 10 μmol/L Y-27632 + 10 ng/mL EGF and injected and isolated from xenograft flank tumors of NSG mice twice. Finally, SmoM2 cells were sorted using FACS (BD FACSAria III machine) for high SMOM2-YFP expression. This final cell stock was used for experiments. CellTiter-Glo 2.0 Cell Viability Assay (Promega, G9248) was used for proliferation and viability assays. Population doubling (14), CRE (7), and TEAD reporters (11) were performed as previously described. For GLI-luciferase, SmoM2 cells in 24-well plates were transfected with 8xGLIBs (168 ng/cm^2). HEK293 cells in 24-well plates were cotransfected with 8xGLIBs (216 ng/cm^2), GLI1 (13 ng/cm^2), and the indicated constructs (26 ng/cm^2). Luciferase activity was measured 4 or 24 hours after transfection using a Dual-Glo Luciferase Assay Kit (Promega, E2940) and a Microtiter plate luminometer (SpectraMax iD3, Molecular Devices LLC). Firefly luciferase was normalized to renilla luciferase in all samples. Unless otherwise stated, cells were treated with 50 μmol/L BAY60-6583, 50 μmol/L isoproterenol, 10 μmol/L forskolin (Cayman Chemical, 11018), 100 μmol/L IBMX (Sigma, I5879), 4 μmol/L VT-104 (Sigma, SML3445), and 20 μmol/L GANT61 (Tocris 3191). HEK293 and Lenti-X 293T cells were obtained directly from the company and not further authenticated. N/TERT2G cells, normal mouse keratinocytes, and SmoM2 cells were validated by short tandem repeat profiling (ATCC Cell Authentication Services). *Mycoplasma* was tested every 6 months by PCR (15), and the cells used did not show contamination.

Staining and immunoblotting

Immunofluorescence, histology, whole mount, and blotting were performed as previously described (16). Whole mount and paraffin embedding methods quench transgene YFP and GFP signals. Slides were imaged on a Leica SP8 confocal microscope with LASX software (RRID:SCR_013673) or with a Keyence BZ-X700 with BZX software. Whole mount β-galactosidase staining was performed as previously described (7). Stained hematoxylin and eosin (H&E) slides were scanned with a NanoZoomer Digital Slide Scanner (Hamamatsu, RRID:SCR_023762). Tumor burden is defined as the total epidermal area divided by the length of the tissue section quantified in H&E sections by the HALO platform (Indica Labs, RRID:SCR_018350). Bands were detected using a ChemiDoc Imaging System (Bio-Rad Laboratories, RRID:SCR_021693) with Clarity Western ECL (Bio-Rad Laboratories). Blot images were processed using Image Lab software, version 5.2.1 (Bio-Rad Laboratories, RRID:SCR_014210). Final images were assembled using Adobe Illustrator version 29.2. Immunoprecipitation was performed as previously described (11) in HEK293 cells, as indicated in the figure legends. All antibodies used are listed in Supplementary Table S2.

Gene expression analysis

Gene expression analysis and single-cell sequencing were performed on isolated tail keratinocytes. For bulk RNA sequencing (RNA-seq), keratinocytes were isolated from SmoM2 mice, mice carrying loxP sites surrounding *Gnas* exon one (abbreviated *Gnas*-eKO), and PKI mice 29, 42, and 57 days after tumor induction, respectively. For single-cell RNA-seq, keratinocytes were isolated from all mice 28 days after tumor induction. *Gpr161*-eKO mice were harvested at 4 months of age. Bulk RNA-seq and quantitative PCR were performed as previously described (11). Primers are shown in Supplementary Table S1. Bulk RNA-seq and Kyoto Encyclopedia of Genes and Genomes (KEGG) pathway enrichment analysis were performed using Partek Flow software, version 12 (Partek, RRID:SCR_011860). Upstream regulators analysis was performed using Ingenuity Pathway Analysis (IPA, Ingenuity Systems, RRID:SCR_008653). For single-cell RNA-seq, tail keratinocytes were isolated from two mice of each genotype. Single-cell isolation and data processing were performed by the CCR Single Cell Analysis Facility. 10x Genomics Chromium Next GEM Single Cell 3′ version 3.1 (Dual Index) was used with a single capture lane per sample. Sequencing was performed by the CCR Sequencing Facility. Single-cell counts were analyzed using Partek Flow software. Cells were filtered by quality measurements, and counts were normalized using counts per million. Normalized counts for each cell were used for unsupervised clustering using principal component analysis, followed by the Harmony batch removal tool (17) and graph-based clustering to identify cell groups. Clustering of groups was performed by creating pseudobulk data in Partek Flow by pooling single cells from each group using the sum of raw counts as the aggregation method. No custom computer code was used in the study.

BCC mutation analysis

Human BCC mutations were identified from a previous database (18). Only coding sequence mutations present in *GNASL* (NM_000516) and *GNASS* (NM_080426) were considered. We predicted the impact of mutations using algorithms available via the Ensembl Variant Effect Predictor (RRID:SCR_007931; ref. 19), including SIFT, PolyPhen2, Mutation Assessor, CADD, AlphaMissense, PrimateAI, SpliceAI, MutationTaster, dbSCSNV, and MutPred. The effect of mutations was further analyzed using the Atlantis webserver (https://atlantis.bioinfolab.sns.it; RRID:SCR_027648).

In vivo microscopy

Skin imaging was performed as previously described (20) in the ear of three mice on days 3 and 17 after induction, using an inverted TCS SP8 DIVE Spectral Microscope (Leica, RRID:SCR_018852) equipped with a Mai Tai tunable laser (Spectra-Physics), two spectral detectors (HyD-RLD, Leica), and a 37°C preheated 40× objective (NA 1.10, HC PL IRAPO, Leica). The specimens were excited at 910 nm. Collagen I (second harmonic generation) and GFP were detected, respectively, at 451 to 461 nm and 504 to 526 nm. For image analysis, surfaces algorithm from Imaris 9.2.1 (Bitplane AG, RRID:SCR_007370) software was used to calculate tumor volume. The measurements point algorithm was used to measure the distance between tumors and hair follicles.

Statistical analysis

The number of independent experiments and statistical tests is indicated in each figure legend. No statistical methods were used to predetermine sample size; sample sizes were chosen based on results from previous studies. Investigators were not blinded to treatment allocation. Statistical analyses were performed using Prism 9 (GraphPad Software, RRID:SCR_002798). Asterisks indicate statistical significance (nonsignificant, ns, $P > 0.05$; *, $P < 0.05$; **, $P < 0.01$; ***, $P < 0.001$; ****, $P < 0.0001$). Drug dose curve fitting and Loewe scores were calculated using Combenefit software (RRID:SCR_027410).

Results

Gαs and PKA inactivation trigger oncogenic Hedgehog signaling

Gαs and PKA inactivation in mouse skin lead to highly proliferative lesions of basaloid cells, which form clumps and islands deeply invading the underlying stroma (7). Although these lesions resemble BCC tumors, it remains unclear how similar they are to those arising from oncogenic activation of the canonical Hedgehog pathway (**Fig. 1A**). To compare tumors, we utilized a series of mouse models with keratin 14 (K14)–inducible Cre recombination (K14CreERT), targeting the epidermal basal compartment (**Fig. 1B**; ref. 21). To trigger canonical oncogenic Hedgehog signaling, we expressed a constitutively active SMOM2 mutant upon Cre recombination (abbreviated SmoM2; ref. 22). The SmoM2 mouse model represents SMO inhibitor–resistant BCC (23). Gαs pathway inactivation was carried out either by knockout of the *Gnas* gene, utilizing *Gnas*-eKO (8), or by overexpression of the PKA-inhibitory domain of PKIα, with mice carrying LoxStopLox-rtTA (24) and tetracycline-inducible PKIα1-24 peptide tagged with GFP (abbreviated PKI). Between 3 and 6 weeks after tumor induction, all three models developed epidermal thickening, primarily on the ears, snout, and paws. These thickened skin areas presented basaloid tumor lesions that invaded the underlying dermis, morphologically resembling superficial and nodular BCC (**Fig. 1C**; refs. 7, 22, 25). Immunofluorescence staining of tail epidermis whole mounts revealed that the BCC-like lesions in the three mouse models were positive for the basal keratinocyte marker K5 and the basaloid skin tumor marker K17 (**Fig. 1D**; ref. 26). Tumor cells in all three models were ciliated, as evidenced by the cilia marker acetylated tubulin (**Fig. 1D**).

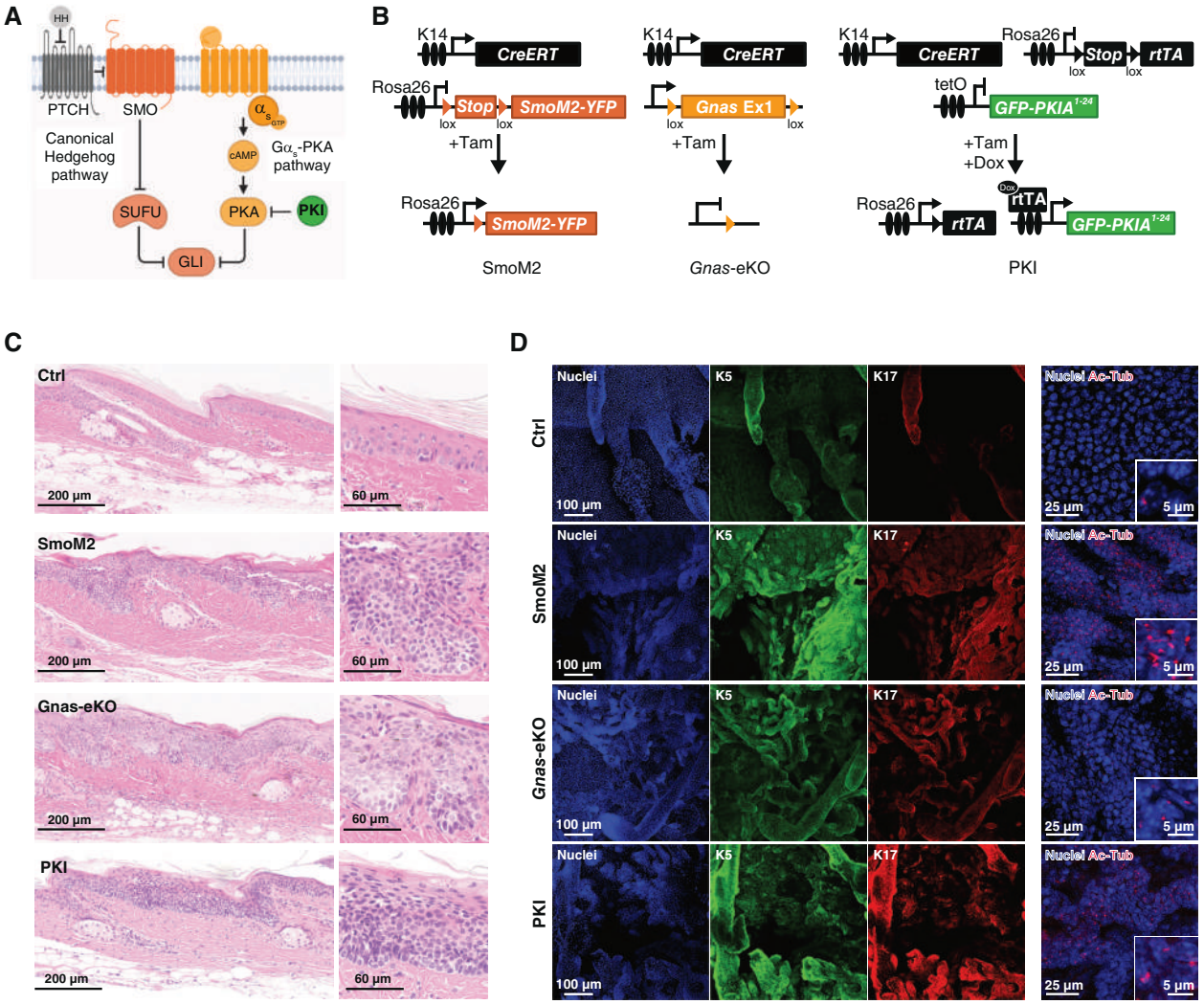

Figure 1.

Both oncogenic Hedgehog and Gαs-PKA inactivation trigger BCC-like tumors in mouse skin. **A,** Model summarizing the canonical Hedgehog pathway and the Gαs-PKA pathway regulating GLI transcription. **B,** Schematic representations of the SmoM2, *Gnas*-eKO, and PKI-inducible mouse models. **C,** Representative images from H&E staining of cross-sections of tail skin from control WT (Ctrl), SmoM2, Gnas-eKO, and PKI mice showing similar BCC tumors, with magnification of the epidermis. **D,** Representative images from immunofluorescence staining of tail skin whole mounts showing expression of the basal marker K5, the BCC marker K17, and the cilia marker acetylated tubulin (Ac-Tub). Created in BioRender. Iglesias, R. (2025) https://BioRender.com/6covj1u.

Bulk RNA-seq of tail keratinocytes from BCC mice revealed similar changes in gene expression among the mouse models, particularly between SmoM2 and *Gnas*-eKO (**Fig. 2A**; Supplementary Fig. S1A). Significantly dysregulated common genes were enriched for pathways related to BCC, including Hippo, TGFβ, and Hedgehog signaling (**Fig. 2B**). Indeed, numerous genes associated with Hedgehog signaling were upregulated in the skin, including *Gli* and *Ptch* (Supplementary Fig. S1B). Functional analysis of transcriptional regulators by IPA indicated upregulation of BCC-related transcriptional networks (Supplementary Fig. S1C).

To better understand the changes triggered by oncogenic Hedgehog signaling, we performed single-cell RNA-seq of tail keratinocytes. Tail skin cell populations were classified by unsupervised clustering and expression of known markers for each cell type (**Fig. 2C**; Supplementary Fig. S1D and S1E; refs. 27–30). Only basal cells were selected for further analysis. Interfollicular stem cells from the mouse tail were divided depending on scale or interscale markers (29). BCC-like cells were identified based on the presence of Hedgehog signaling markers (*Gli1-2-3*, *Ptch1-2*, *Smo*, and *Gas1*) and an increased cell number for that population in BCC models (**Fig. 2D**). We confirmed that cells in *Gnas*-eKO mice had reduced *Gnas* expression and that *Gnas* depletion was enriched in BCC cell populations (Supplementary Fig. S1F).

Remarkably, SmoM2, *Gnas*-eKO, and PKI mice presented highly similar cell profiles and upregulation of Hedgehog targets (**Fig. 2E–G**). BCC-like cells clustered in two separate populations, BCCA and

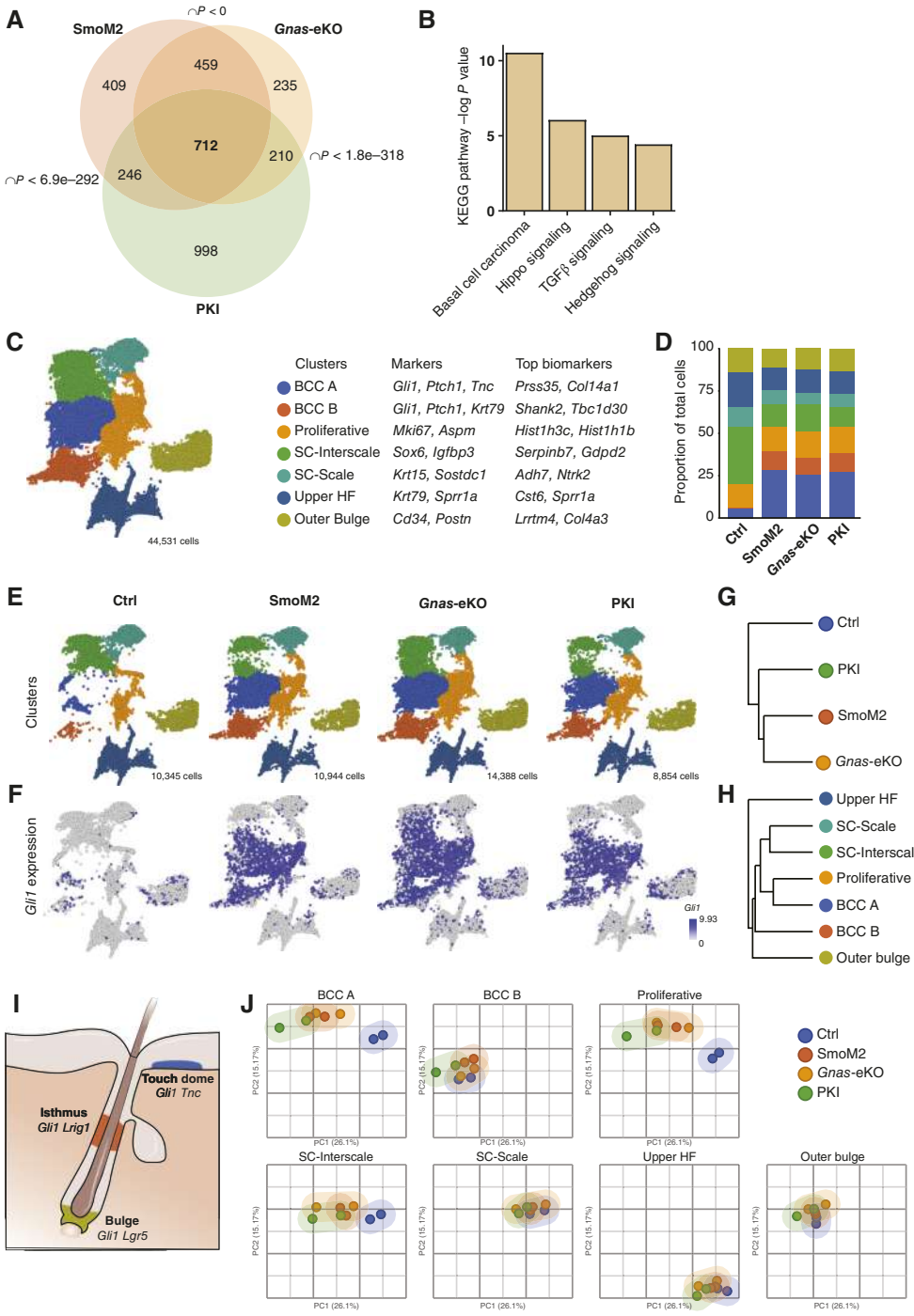

Figure 2.

SMO and Gαs/PKA inactivation trigger oncogenic Hedgehog signaling. **A,** Venn diagram showing the differentially regulated gene overlap between mouse models by bulk mRNA-seq ($q < 0.05$, $|FC| \geq 1.5$). *P*, *P* value of the overlap, Fisher exact test. $N = 4$ for each of SmoM2, *Gnas*-eKO, and PKI mice; $N = 9$ for control mice. **B,** Graph indicating the enriched KEGG pathway terms in the 712 overlapping genes shown in **A**. **C,** Uniform Manifold Approximation and Projection (UMAP) plot of cell clusters from all mouse models from tail single-cell sequencing. Gene markers used for cell identification and top enriched biomarkers for each cluster are indicated. $N = 2$ mice per genotype, 44,531 total cells. HF, hair follicle; SC, stem cell. **D,** Relative proportion of each cell population shown in **C** for each mouse model. **E,** UMAP of cell clusters for each mouse model. $N = 2$ mice per genotype. The number of cells sequenced is indicated. **F,** Expression of *Gli1* projected into each UMAP. **G** and **H,** Unsupervised hierarchical clustering of pseudobulk single-cell RNA-seq data based on mouse genotype (**G**) or cell cluster (**H**). **I,** Schematic showing *Gli*+ stem cell compartments in skin. **J,** Principal component (PC) analysis plots showing clustering of the different cell populations for each mouse, calculated with pseudobulk single-cell RNA-seq data based on mouse genotype and cell cluster.

BCCB, that matched cell clusters present in control mice (**Fig. 2E**). The BCC-like cells in control mice corresponded to *Gli*+ populations (**Fig. 2E** and **F**). The gene expression profile of BCCA cells was closely related to the proliferative compartment and basal stem cells (**Fig. 2H**), possibly indicating a higher proliferative potential for these cells. GLI is present in three main stem cell areas in normal skin (**Fig. 2I**). Based on markers for these GLI+ stem cells, we hypothesize that BCCA cells correspond to a touch dome stem cell–like state (*Tnc*+), whereas BCCB matches an isthmus stem cell phenotype (*Krt79*+) although both populations present broad expression of hair follicle stem cell markers such as *Lgr5* and *Lrig1* (Supplementary Fig. S1D and S1E).

The populations with more changes in their RNA profile corresponded to BCC-like cells, the proliferative compartment, and

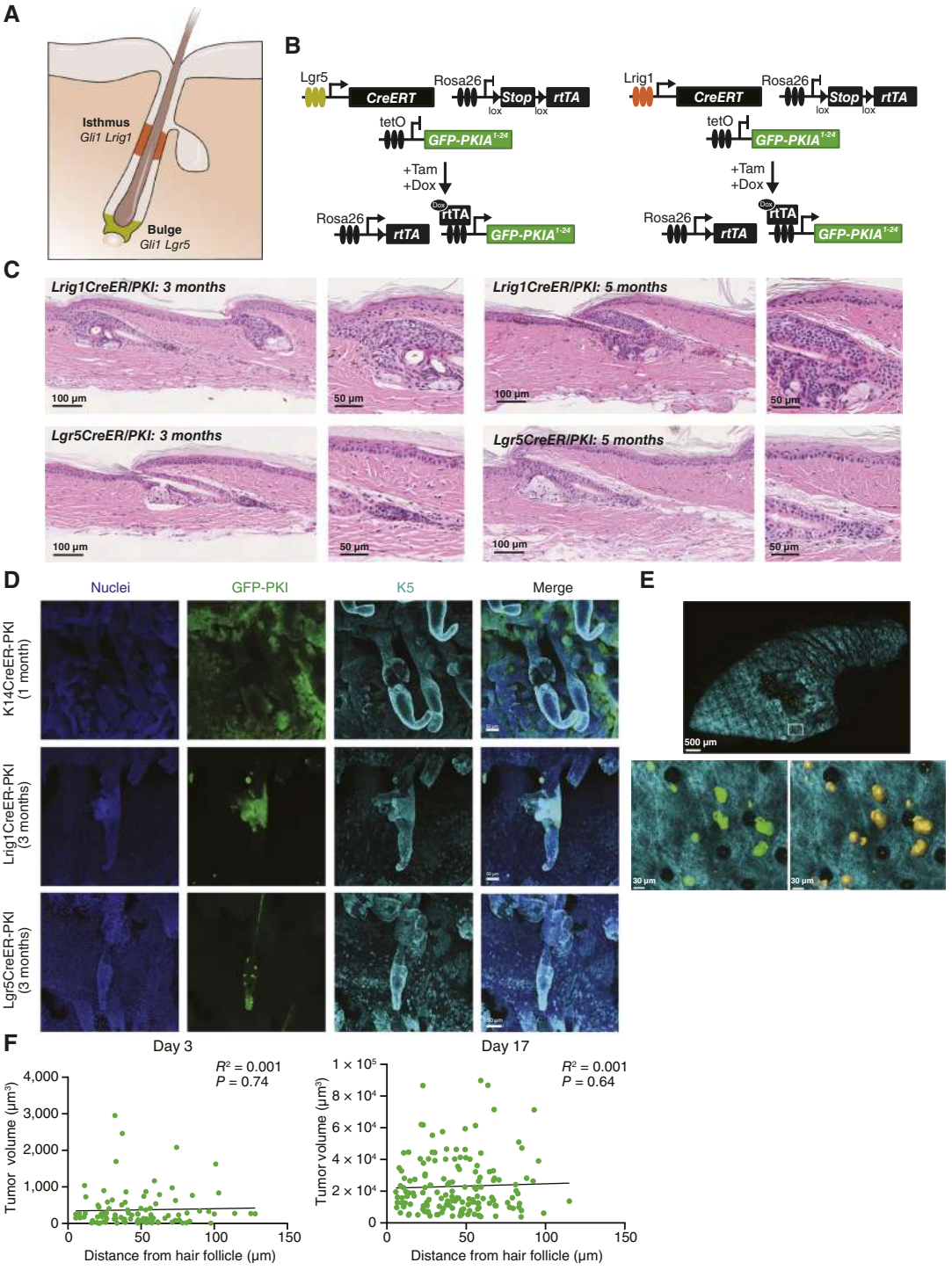

Figure 3.

Hair follicle stem cells have limited potential to generate BCC-like tumors. **A,** Schematic showing bulge and isthmus stem cell compartments in skin. **B,** Schematic representations of the mice used to target PKA inactivation to hair follicle stem cell compartments. **C,** Representative images from H&E staining of tail skin from the indicated mice 3 and 5 months after induction. **D,** Representative images from immunofluorescence staining of tail skin whole mounts showing expression of PKI and the basal marker K5 at the indicated time after induction. **E,** Two-photon images of a mouse whole ear with GFP-PKI tumors (green) and collagen (cyan) visualization from a mouse 17 days after induction. Magnified images show GFP-PKI tumors. Hair follicles can be visualized by disruptions in the collagen (black circular areas). Right, a rendering for tumor volume analysis (Imaris) used for quantification is shown. **F,** Quantification of the distance between tumors and the closest hair follicle. Each dot represents an individual tumor. Day indicates the days after tumor induction. The best fit regression line is shown. Day 3, $N = 98$ tumors from three mice; day 17, $N = 155$ tumors from three mice.

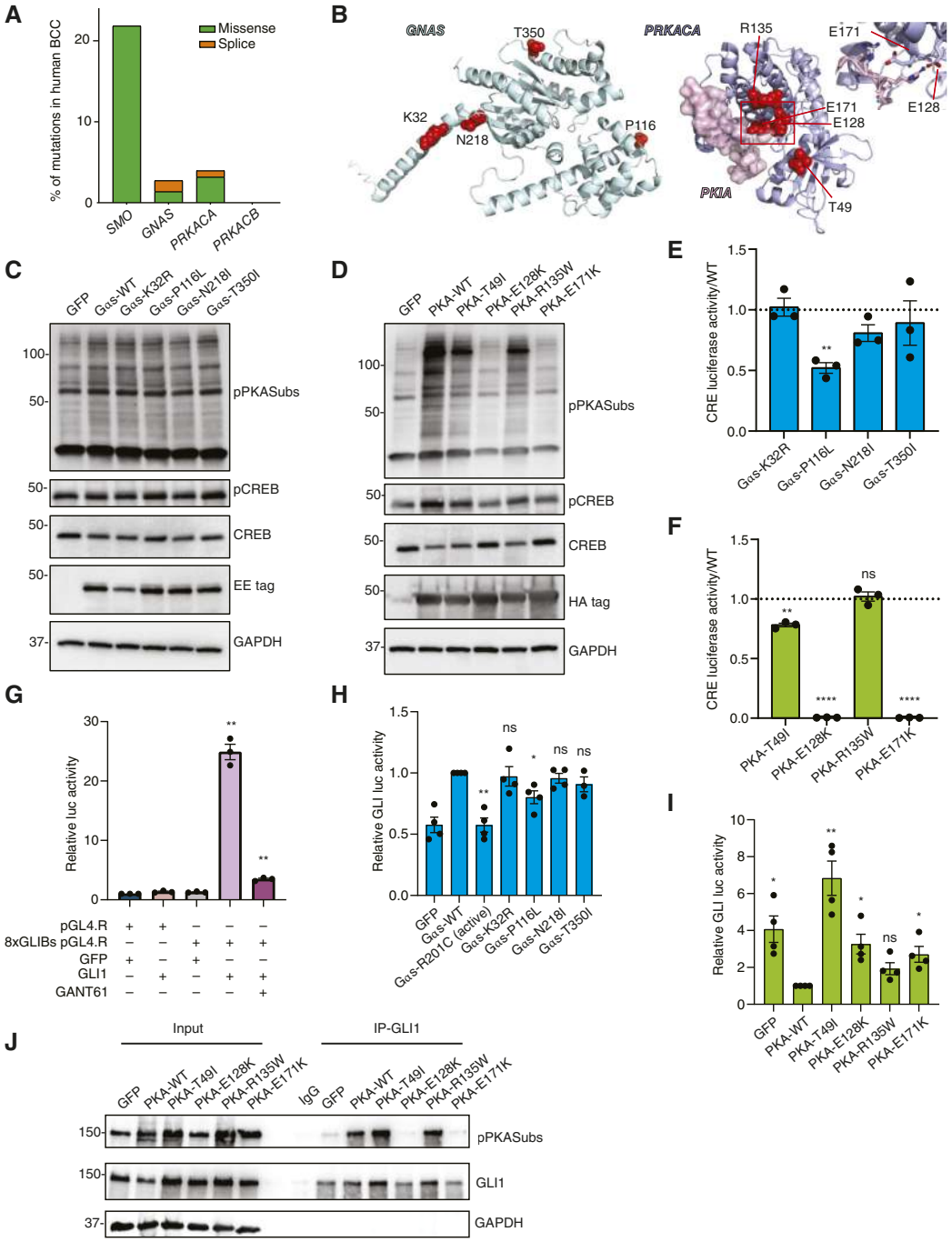

Figure 4.

Gαs and PKA inactivating mutations are present in human BCC. **A,** Prevalence of indicated gene mutations in human BCC. *SMO* and *GNAS* mutations, $N = 293$ tumors; *PRKACA*, $N = 126$ tumors. **B,** Protein models of Gαs (*GNAS*) and PKACα (*PRKACA*), with mutated amino acids highlighted in red. PKA is shown in complex with the pseudo-substrate PKIA. Magnification on the right shows amino acids important for substrate interaction between PKA and PKI. **C** and **D,** Western blot analysis of the expression of EE-tagged Gαs (**C**), HA-tagged PKA (**D**), WT, or mutants and downstream signaling pathway components in transfected HEK293 cells. pPKASubs, Phospho-PKA Substrate RRXS*/T*. Molecular weight markers (kDa) are indicated on the left. **E** and **F,** Transcriptional activity of CREB measured by CRE-luciferase assay in HEK293 cells transfected with Gαs (**E**) or PKA (**F**) variants. Graphs show mean ± SEM. The dotted line indicates the activity level of WT transfected samples. In **E**, $N = 3$, one-sample Wilcoxon test; in **F**, $N = 3$, one-sample Wilcoxon test. **G,** Luciferase assay in HEK293 cells transfected with the indicated constructs (+). Graphs show mean ± SEM. $N = 3$, one-sample Wilcoxon test. **H** and **I,** Transcriptional activity of GLI in HEK293 cells transfected with GLI-luciferase reporter, GLI1, and Gαs (**H**) or PKA (**I**) variants. Graphs show mean ± SEM. In **H**, $N = 3$ for Gαs-T350I and $N = 4$ for all other constructs, one-sample Wilcoxon test; in **I**, $N = 4$, one-sample Wilcoxon test. **J,** Western blot analysis indicating phosphorylation of GLI1 by PKA in HEK293 cells transfected with PKA variants and GLI1. GLI1 was immunoprecipitated and tested with anti–phospho-PKA substrate motif antibody (pPKA-subs). ns, nonsignificant; *, $P < 0.05$; **, $P < 0.01$.

interscale stem cells (SC-Interscale) based on clustering analysis of pseudobulk samples (**Fig. 2J**). This was not necessarily a reflection of changes in the proportion of total cells for those populations as the BCC-like cells expanded in SmoM2, *Gnas*-eKO, and PKI mice, with a decrease in the number of SC-Interscale, whereas the proportion of proliferative cells did not change (**Fig. 2D**).

Overall, our results establish that tumor cells arising from Gαs pathway inactivation are almost indistinguishable from those resulting from canonical oncogenic Hedgehog pathway activation. We also find that BCC-like tumor cells have gene expression profiles similar to those of touch dome and isthmus basal stem cells. Remarkably, the main gene expression changes triggered by oncogenic Hedgehog signaling are reflected in the BCCA and proliferative cells, whereas oncogenic activation does not significantly alter other stem cell compartments.

Hair follicle stem cells have limited potential to generate BCC-like tumors

Bulk and single-cell RNA-seq confirmed the similarity of BCC-like lesions to hair follicle stem cells, suggesting a hair follicle origin for these tumors. However, by reprogramming toward a hair follicle phenotype (31), BCC could originate from other keratinocyte stem cell populations. To better characterize the origin of BCC-like cells, we analyzed the tumorigenic potential of different hair follicle stem cell populations by crossing our inducible PKI transgene with drivers specific for isthmus *Lrig1* (32) or bulge *Lgr5* (33) hair follicle stem cells (**Fig. 3A** and **B**). Remarkably, *Lgr5* cells were unable to drive tumor formation (**Fig. 3C**). In contrast, *Lrig1* cells formed lesions limited to the mid-hair follicle area (**Fig. 3C**). These *Lrig1*-derived tumors did not migrate into the interfollicular epidermis or invade the dermis, as observed with the K14 driver. We validated that GFP-PKI is expressed in specific hair follicle compartments by staining tail epidermis whole mounts against GFP (**Fig. 3D**). Our results indicated that *Lrig1* and *Lgr5* hair follicle stem cells are unlikely to be the primary origin of BCC-like invasive tumors following PKA inactivation.

To better understand tumor origin and evolution in our BCC model, we took advantage of the GFP fluorescent protein fused to PKI to track BCC-like tumors by two-photon microscopy in K14-driven mice. Utilizing second-harmonic generation to image collagen (34), we can also observe the tissue structure and track the location and growth of tumors according to their distance from the hair follicle (**Fig. 3E** and **F**). Our results indicate that tumor formation (day 3) and tumor growth (day 17) have no significant correlation with the distance to the hair follicle (**Fig. 3F**), supporting that despite their hair follicle stem cell phenotype, a proportion of BCC-like cells may not originate from hair follicles themselves.

Gαs and PKA inactivating mutations are present in human BCC

The similarity between our tumor models suggests that genomic alterations in Gαs-PKA signaling members could contribute to the genetic risk of Hedgehog-driven tumors. Analysis of a tumor dataset of human BCC (18) shows mutations in genes coding for Gαs and PKA (**Fig. 4A** and **B**). Mapping and effect predictor analysis of mutations indicated potentially altered protein activity for some variants (Supplementary Table S3). Notably, two mutations in the PKA catalytic subunit alpha (*PRKACA*) are in residues that are essential for the kinase to interact with substrates (E128 and E171, **Fig. 4B**). To test the biological effect of the mutations, we measured the activity of Gαs and PKA variants present in BCC. Although Gαs mutants showed similar activity levels to WT, all PKA mutations reduced phosphorylated PKA substrates and cAMP-responsive element binding protein (CREB) phosphorylation (**Fig. 4C** and **D**). We next utilized a CRE-luciferase reporter that indicates the activity of the cAMP pathway by measuring CREB transcription. Interestingly, one *GNAS* variant, Gαs-P116L, showed reduced CREB reporter activation (**Fig. 4E**). The *PRKACA* variants PKA-E128K and E171K completely abolished the activation of the CREB reporter, and PKA-T49I showed reduced activity (**Fig. 4F**).

To test the effect of these mutants on Hedgehog signaling, we developed a reporter with repeated GLI binding sites (12) followed by luciferase (8xGLIBs). The 8xGLIBs reporter, but not an empty reporter vector, responded to GLI1 overexpression, and this response was blocked by the GLI inhibitor GANT61 (**Fig. 4G**). WT Gαs or BCC mutants had a limited effect on GLI1 activity, whereas a constitutively active Gαs (R201C) was able to block its transcription (**Fig. 4H**). On the contrary, overexpression of WT PKA inhibited GLI1, but three PKA variants (T49I, E128K, and E171K) resulted in increased GLI1 transcription (**Fig. 4I**). PKA can control the activity of GLI by regulating its phosphorylation (35). Indeed, we find that WT PKA increases GLI1 phosphorylation, whereas the PKA variants E128K and E171K show a reduced effect (**Fig. 4J**). Remarkably, PKA-T49I increases GLI1 transcriptional activity without altering its phosphorylation (**Fig. 4I** and **J**), suggesting alternative mechanisms by which PKA could regulate GLI. Our results show that disruptive mutations in Gαs and PKA are present in human BCC samples and indicate that inactivation of this pathway may contribute to human BCC.

BCC tumors arising from Gαs pathway inactivation are independent of the canonical Hedgehog regulators SMO and GPR161

Gαs and PKA are necessary to block Hedgehog signaling during normal epithelial differentiation, suggesting that potential Gαs-coupled GPCRs are involved in the regulation of stem cell fate in the skin. Analysis of our gene datasets identified numerous GPCRs expressed in tumor cells from our mouse models (**Fig. 5A**, magnified for clarification in Supplementary Fig. S2). Interestingly, GPCRs that regulate Hedgehog signaling, such as *Smo* and *Gpr161*, are present in BCC-like cells (Supplementary Fig. S3A).

Although it is known that PKA acts directly on GLI transcription factors to regulate the Hedgehog pathway (2), one open question is whether oncogenic Hedgehog signaling following Gαs and PKA inactivation depends on SMO. To test this possibility, we performed a skin-specific double knockout of *Smo* and *Gnas* or a knockout of *Smo* in the context of PKI expression (**Fig. 5B**; Supplementary Fig. S3B). Surprisingly, *Smo* knockout did not alter tumor formation or Hedgehog signaling activation in *Gnas*-eKO or PKI mice (**Fig. 5B–D**; Supplementary Fig. S3B–S3D). Furthermore, we found that tumor growth following PKI expression is resistant to the SMO inhibitor vismodegib (Supplementary Fig. S3E), validating that these BCC-like lesions do not depend on SMO for growth.

Combined with our previous study demonstrating that Gαi-GPCR activation does not lead to BCC (16), our *Smo* knockout results suggest that a Gαs-coupled receptor must be present in the skin, which inactivates Hedgehog signaling during normal

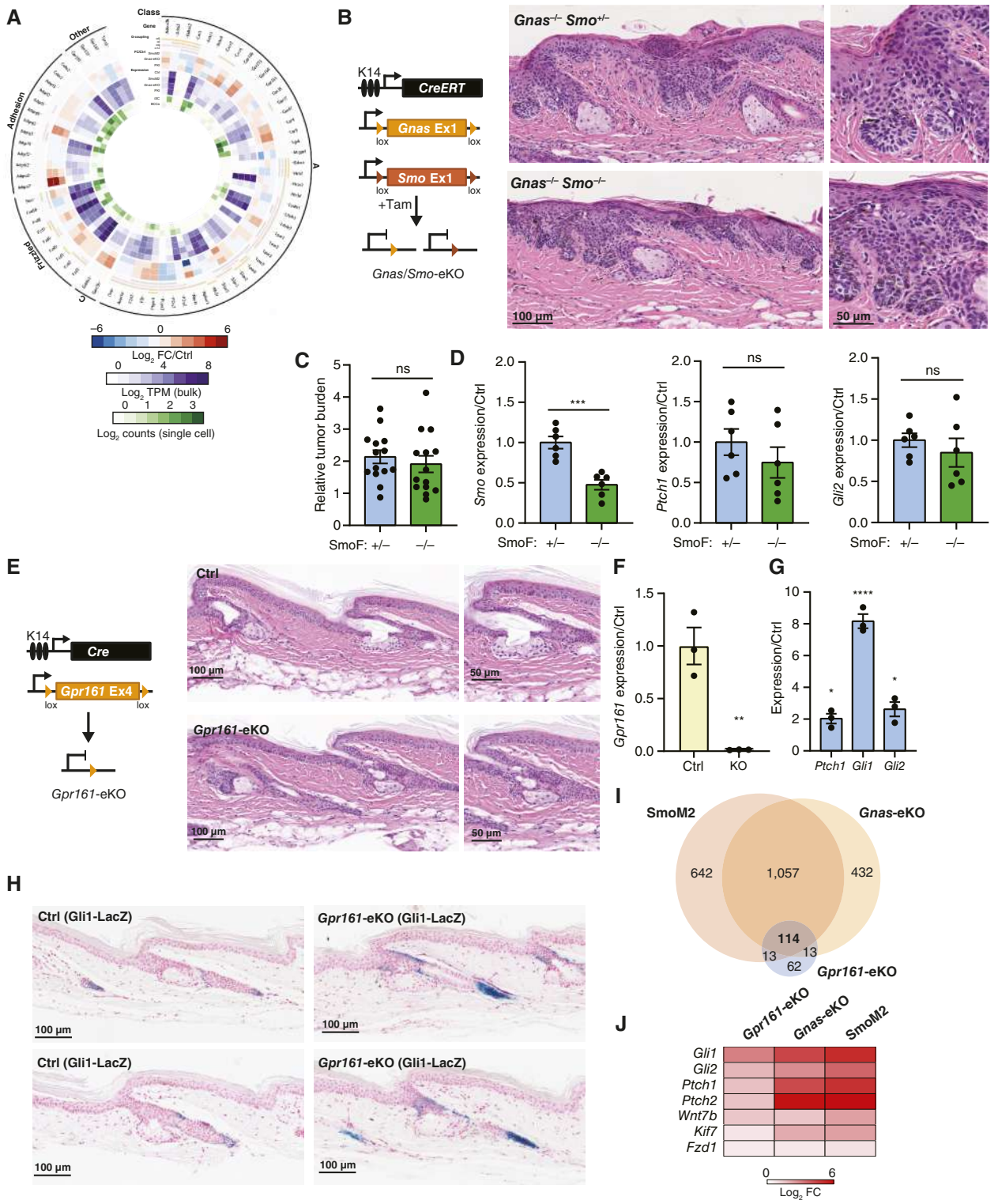

Figure 5.

BCC tumors arising from Gαs pathway inactivation are independent of canonical Hedgehog regulators. **A,** Circos plot representing BCC GPCR expression in mice, showing class, gene name, Gα coupling, fold change (FC), and expression level (log_2 of transcripts per million, TPM) in bulk RNA-seq and level of expression in single-cell RNA-seq (log_2 counts) in SC-Interscale (iSC) and BCCA clusters. See the amplified image in Supplementary Fig. S2. **B,** Schematic representation of the mouse model used to target Gαs and SMO deletion to the skin. Images on the right show representative H&E staining of tail skin from the indicated mice 33 days after induction. −/+, heterozygous knockout; −/−, homozygous knockout. **C,** Quantification of tumor burden per mouse (*Continued on the following page.*)

homeostasis. We hypothesized that if the effect is mediated by a single GPCR, skin-specific knockout of this receptor would phenocopy *Gnas*-eKO BCC. A literature review of skin-specific or complete knockouts of the Gαs-coupled receptors expressed in BCC cells did not identify any receptor in which absence results in BCC-like lesions. However, *Gpr161* and *Adgra2* (also known as *Gpr124*) emerged as potential candidates. *Gpr161* is a Gαs-coupled receptor and one of the primary inhibitors of Hedgehog signaling during development and tumor formation (2, 36, 37), whereas *Adgra2* is the most upregulated GPCR in BCC cells (**Fig. 5A**). The complete knockout of these receptors is embryonically lethal (10, 36), and their specific skin knockout has not yet been analyzed. Interestingly, *Adgra2* skin-specific knockout mediated by constitutive CRE recombination (K14Cre; ref. 21) and lox-p sites on *Adgra2* exon 1 (10) did not affect skin homeostasis (Supplementary Fig. S4A–S4C).

Next, we analyzed GPR161. To confirm that this receptor can regulate Hedgehog signaling in keratinocytes, we generated inducible keratinocyte cell lines overexpressing WT or V129E GPR161, a mutation that abolishes GPR161 interaction with Gαs (36). Overexpression of WT but not mutant GPR161 leads to the expression of GLI3 repressor and activation of CREB (Supplementary Fig. S4D and S4E), indicating that GPR161 can regulate Hedgehog signaling in keratinocytes. Surprisingly, however, inducible (K14CreERT) or constitutive (K14Cre) skin-specific knockouts utilizing a floxed *Gpr161* mouse (9) did not show any phenotypic or histologic alterations (**Fig. 5E** and **F**; Supplementary Fig. S4F–S4H).

Analysis of Hedgehog targets in *Gpr161* knockout tail skin keratinocytes indicated that despite the lack of phenotype, keratinocytes show increased expression of Hedgehog targets (**Fig. 5G**). Using *Gli1* β-galactosidase reporter mice (*Gli1*^{lacZ}; ref. 38), we were able to visualize that *Gpr161* epithelial knockout led to an increase in *Gli1*+ cells limited to the hair follicle (**Fig. 5H**). Comparison of bulk RNA-seq analysis of *Gpr161* tail skin keratinocytes with SmoM2 and *Gnas*-eKO mice indicated that fewer genes were differentially regulated by *Gpr161* knockout although several of these genes were shared (**Fig. 5I**). *Gpr161* epithelial knockout leads to a less pronounced increase in Hedgehog target genes compared with SmoM2 and *Gnas*-eKO (**Fig. 5J**). Our results show that *Gpr161* knockout in basal keratinocytes leads to a non-oncogenic increase in Hedgehog signaling, suggesting that GPR161 only partially controls the Hedgehog pathway in the skin.

Overall, our GPCR analysis indicates that the tumor-suppressive function of Gαs is probably not linked to a single Gαs-coupled GPCR but might involve multiple upstream receptors. On the other hand, our results demonstrate that BCC tumors arising from Gαs pathway inactivation are independent of the canonical Hedgehog regulators SMO and GPR161 and establish *Gnas*-eKO/PKI models as a unique resource to understand BCC arising from SMO-independent Hedgehog signaling.

Activation of Gαs-coupled ADORA2B reduces BCC tumor growth

As Gαs and PKA are essential inhibitors of the Hedgehog pathway in the skin, elevating cAMP levels and activating PKA could be a viable option to block oncogenic Hedgehog signaling (**Fig. 6A**). Inhibitors of phosphodiesterases (PDE), the enzymes mediating the degradation of cAMP, can suppress Hedgehog signaling and medulloblastoma growth in mouse models (39). However, we found that systemic delivery of the PDE4 inhibitor rolipram, the PDE7 inhibitor BRL50481, or their combination did not affect the growth of SmoM2-induced tumors (**Fig. 6B** and **C**).

Another potential way to increase cAMP levels in cells is to activate Gαs-coupled GPCRs (**Fig. 6A**). Analysis of gene expression in our single-cell BCC data revealed several targetable Gαs-coupled GPCRs present in tumor cells (**Fig. 6D**). As a proof of concept to induce Gαs-coupled GPCR signaling and reduce Hedgehog activity, we utilized BAY60-6583 (40), an agonist for ADORA2B, and isoproterenol, which activates β-adrenergic receptors (ADRB1 and ADRB2). Treatment of a cell line generated from SmoM2 mice with BCC-like characteristics (Supplementary Fig. S5A–S5F) showed activation of PKA signaling following treatment with BAY60-6583 or isoproterenol (**Fig. 6E**). Furthermore, this treatment led to reduced mRNA expression of Hedgehog signaling targets, such as *Gli1* and *Gli2* (**Fig. 6F**), as well as GLI1 protein expression (**Fig. 6G**) and reduced cell proliferation (Supplementary Fig. S5G). However, BAY60-6583 showed a more acute and sustained inhibition of endogenous GLI transcriptional activity than isoproterenol (**Fig. 6H**). Gαs and PKA can regulate cell growth in BCC not only by regulating GLI but also by blocking the activity of YAP1 (7, 13). Using a TEAD transcription reporter assay that measures the activity of YAP1, we found that BAY60-6583 blocks endogenous YAP1-TEAD activity to a similar extent as the YAP1 inhibitor VT-104, whereas isoproterenol had no effect (**Fig. 6I**). Interestingly, we also found that the ADORA2B receptor can localize to cilia in some SmoM2 cells (**Fig. 6J**). We were able to validate that BAY60-6583 can block human GLI1 transcriptional activity and increase GLI1 phosphorylation by PKA in HEK293 cells (Supplementary Fig. S5H and S5I).

To extend our results in an *in vivo* setting, we treated SmoM2 mice with daily topical application of BAY60-6583 or isoproterenol for 10 days, 3 weeks after tumor induction. Surprisingly, and aligned with our *in vitro* data, BAY60-6583 reduced tumor burden, whereas isoproterenol did not significantly alter tumor growth (**Fig. 6K** and **L**). BAY60-6583 significantly reduced tumor cell proliferation (**Fig. 6M** and **N**). The discrepancy in the effects between BAY60-6583 and isoproterenol could arise from their differential regulation of Hedgehog and Hippo

(*Continued*.) in H&E tail skin staining in *Gnas* skin knockout mice with *Smo* heterozygous (+/−) or homozygous (−/−) knockout. Graphs show mean ± SEM. $N = 14$ SmoF +/− mice; $N = 14$ SmoF −/− mice, *t* test. **D,** qRT-PCR analysis of mRNA expression of indicated markers in tail epidermal keratinocytes isolated from *Gnas* knockout mice with *Smo* heterozygous (+/−) or homozygous (−/−) knockout 33 days after induction. Graphs show mean ± SEM. $N = 6$ SmoF +/− mice; $N = 6$ SmoF −/− mice, *t* test. SmoF ± mice were used as control (Ctrl). **E,** Schematic representation of the mouse model used to target *GPR161* deletion to the skin. Images on the right show representative H&E staining of tail skin from the indicated mice at 4 months. **F** and **G,** qRT-PCR analysis of mRNA expression of indicated markers in tail epidermal keratinocytes isolated from 4-month-old control or *Gpr161*-eKO mice. Graphs show mean ± SEM. $N = 3$ control mice and $N = 3$ *Gpr161*-eKO mice; *t* test (**F**) and one-sample Wilcoxon test (**G**). **H,** Representative image of β-galactosidase staining in tail skin from 12-week-old control and *Gpr161*-eKO (K14-Cre) mice showing *Gli*$^{+}$ cells (blue). **I,** Venn diagram showing the differentially regulated gene overlap between indicated mouse models by bulk mRNA-seq ($q < 0.05$, $|FC| \geq 1.5$). SmoM2 and *Gnas*-eKO are K14-CreERTM as shown in **Fig. 2A**, and *Gpr161*-eKO are from K14Cre 4-month-old mice, $N = 3$ control and 3 *Gpr161*-eKO mice. **J,** Heat map from bulk mRNA-seq data comparing the fold change (log_2FC) increase in Hedgehog signaling targets in the indicated mice. ns, nonsignificant; *, $P < 0.05$; **, $P < 0.01$; ***, $P < 0.001$; ****, $P < 0.0001$.

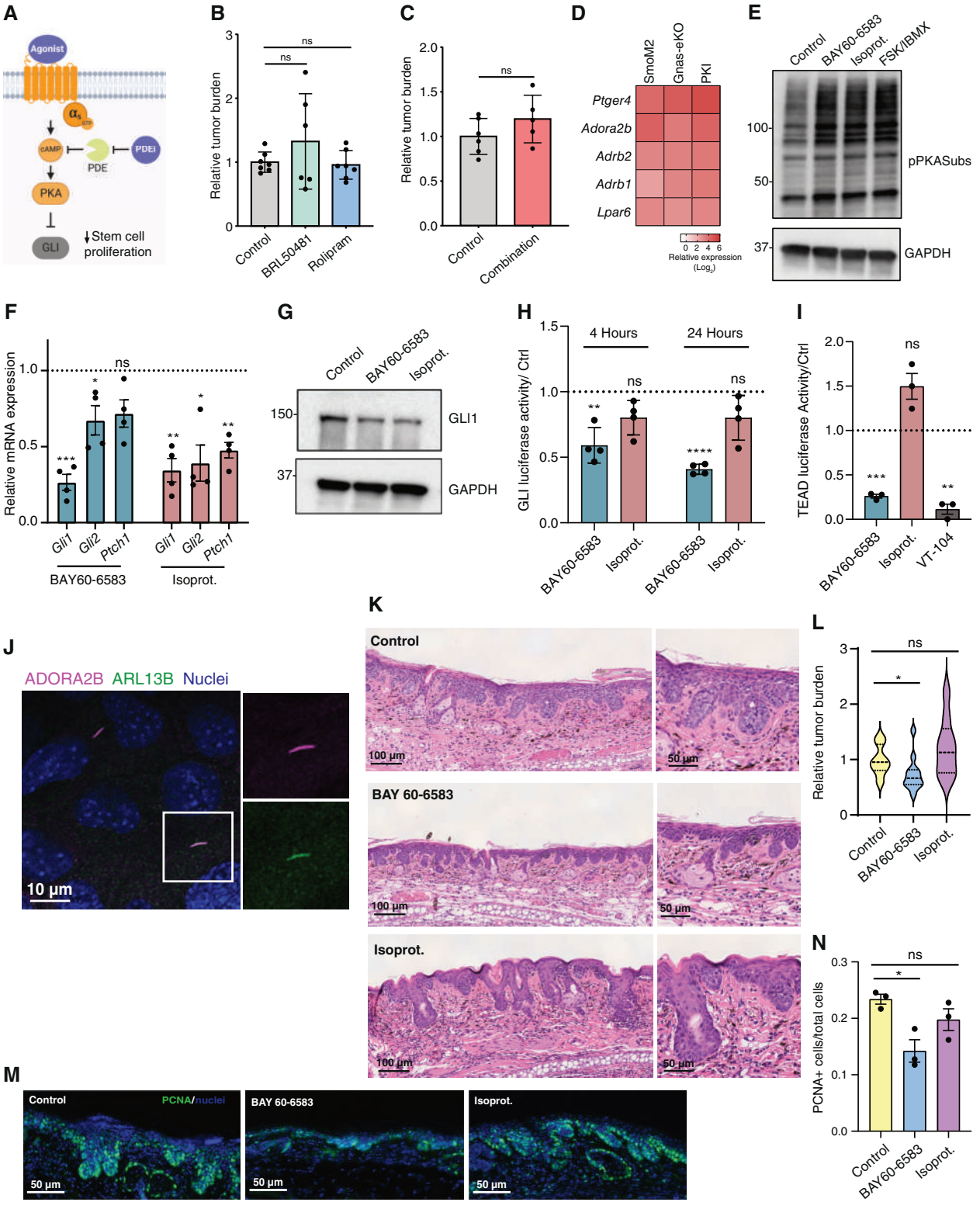

Figure 6.

Activation of Gαs-coupled receptors reduces BCC tumor formation. **A,** Model summarizing the Gαs-PKA pathway and potential therapeutic interventions. **B** and **C,** Quantification of tumor burden per mouse in H&E tail skin from SmoM2 mice treated with BRL50481 or rolipram (**B**) or a combination of both (**C**). Graphs show mean ± SEM. $N = 7$ control, 6 BRL50481, 7 rolipram-treated mice, ANOVA with t test (**B**); $N = 6$ control, (*Continued on the following page.*)

signaling, as shown above, although additional effects could be mediated by their respective receptors being differentially expressed across stem cell compartments in the epidermis (Supplementary Fig. S5J). In addition, *Adora2b* expression is increased in tumor cells in BCC mice compared with control mice, whereas ADRB2 is reduced (Supplementary Fig. S5J).

We also investigated the potential benefit of combining BAY60-6583 with agents targeting Hedgehog signaling in control and BCC keratinocytes. Interestingly, SmoM2 cells were more sensitive to BAY60-6583 treatment than control cells, whereas the opposite was observed for the SMO inhibitor vismodegib (Supplementary Fig. S6A–S6C). Combination analysis revealed limited synergism between the two drugs (Supplementary Fig. S6C and S6D). This is expected as the SMO variant present in our BCC model confers a markedly reduced sensitivity to vismodegib (23), and we show now that this resistance is not altered by ADORA2B activation. Similarly, cotreatment with the GLI inhibitor GANT61 also showed minimal synergistic effects (Supplementary Fig. S6E–S6G). Neither vismodegib nor GANT61 produced additive or synergistic effects with BAY60-6583 on GLI transcriptional activity (Supplementary Fig. S6H). The lack of synergism could indicate that ADORA2B activation affects BCC growth through mechanisms converging on the Hedgehog/GLI pathway and supports a model in which activation of the Gαs-coupled receptor ADORA2B suppresses oncogenic Hedgehog signaling and tumor growth.

Discussion

Oncogenic and dysregulated Hedgehog signaling contribute to numerous human pathologies, including cancer. Here, we dissect the role of Gαs and PKA in the regulation of mammalian Hedgehog, and we demonstrate that inactivation of Gαs and PKA is sufficient to trigger oncogenic Hedgehog signaling at the same level and with the same biological consequences as constitutively active SMO. We also determine that tumors arising from Gαs pathway inactivation are independent of the canonical Hedgehog regulators SMO and GPR161 and establish the *Gnas*-eKO and PKI models as a unique resource to understand tumor formation arising from noncanonical activation of Hedgehog signaling.

Our results indicate that continuous activation of Gαs and PKA is essential to maintain normal levels of Hedgehog activity in the skin stem cell compartment and that this function is epistatic to SMO, supporting the idea that SMO primarily regulates the inhibitory effect of PKA on Hedgehog signaling. Indeed, SMO activity is believed to be predominantly mediated by direct inhibition of PKA through a pseudo-substrate site (41), and Hedgehog pathway hyperactivity is independent of SMO in other models of cAMP signaling inactivation (36, 42, 43), highlighting the overlapping relationship between Gαs, PKA, and Hedgehog signaling.

Despite the hair follicle characteristics of BCC, experimental data in mice indicate that tumors can originate from both inside and outside the hair follicle (31, 44, 45). Here, we demonstrate that BCC-like cells cluster in two distinct populations with markers for touch dome and isthmus stem cell–like cells. Interestingly, we find that although bulge *Lgr5*+ stem cells are not able to generate BCC-like tumors, *Lrig1*+ isthmus stem cells have a limited capacity to generate invasive BCC lesions. These results suggest that BCC-like tumors originate from both hair follicle and interfollicular stem cells, as has been shown before (45–47). However, in our model, more invasive tumor lesions arise outside the hair follicle, probably from touch dome stem cell–like cells. Touch dome *Gli*+ cells express broad interfollicular and hair follicle stem cell characteristics, similar to BCCA cells, and have been proposed as an origin of BCC lesions (30, 45). On the other hand, BCCB cells express high levels of *Krt79*, an epithelial differentiation marker (48), indicating that BCCB could represent a more differentiated tumor population.

BCC has been classically characterized by genomic alterations in Hedgehog signaling members although BCCs present a multiplicity of genetic changes (3, 49, 50). In addition, some patients with high-frequency BCCs do not show germline mutations in the Hedgehog pathway (50, 51), indicating that additional alterations may drive BCC formation. Our results show disruptive mutations in Gαs and PKA in human tumors, suggesting that they could contribute to human BCC. However, the low burden of Gαs and PKA genomic alterations indicates that additional genetic and signaling mechanisms might exist in BCC to inactivate Gαs and PKA. Bazex–Dupré–Christol syndrome, a rare disease that presents with multiple BCCs, has been linked to amplifications in the *ARHGAP36* gene (52). ARHGAP36 can antagonize PKA and activate Hedgehog signaling (53), establishing ARHGAP36 amplification as an alternative pathway to achieve PKA inactivation in BCC. Further research is needed to unveil additional mechanisms by which Gαs pathway inactivation contributes to human BCC and other tumors.

PKA activation has been proposed as a therapy to block oncogenic Hedgehog signaling, although this has not been studied in detail in skin BCC. Here, we find that blockage of cAMP degradation by PDE inhibitors does not affect the growth of SmoM2-induced tumors, but activation of the Gαs-coupled ADORA2B can lead to reduced tumor burden and proliferation. We also find potential differences between Gαs-coupled GPCR agonists, which could arise due to specific activation of particular pools of cAMP/PKA and selective receptor desensitization. Although we find that ADORA2B can be located in cilia, its GLI-

(*Continued*.) 5 combination treated mice, ANOVA with *t* test (**C**). **D,** Heatmap from single-cell RNA-seq data from BCCA cells comparing the relative expression of the indicated Gαs-coupled GPCRs. **E,** Western blot analysis of the SmoM2 BCC cell line showing activation of PKA by treatment with 50 μmol/L BAY60-6583 or isoproterenol (Isoprot.) for 15 minutes. Forskolin and IBMX (FSK/IBMX) treatment is used as a positive control. Molecular weight markers (kDa) are indicated on the left. **F,** qRT-PCR analysis of mRNA expression of indicated markers in a SmoM2 cell line treated with 50 μmol/L of the indicated drugs for 24 hours. Graphs show mean ± SEM. $N = 4$ samples per condition, one-sample Wilcoxon test. The dotted line indicates the expression level of control samples. **G,** Western blot analysis of GLI1 in SmoM2 cell lines treated with 25 μmol/L of the indicated drugs for 72 hours. Molecular weight markers (kDa) are indicated on the left. **H,** GLI-luciferase assay in SmoM2 cells treated with 50 μmol/L of the indicated drugs for 4 and 24 hours. Graphs show mean ± SEM. The dotted line indicates the level of control samples. $N = 4$, one-sample Wilcoxon test. **I,** Transcriptional activity of TEAD measured by TEAD-luciferase assay in SmoM2 cells treated with 50 μmol/L of BAY60-6583 or isoproterenol, and 4 μmol/L of VT-104 (TEAD inhibitor) for 24 hours. Graphs show mean ± SEM. The dotted line indicates the level of control samples. $N = 3$, one-sample Wilcoxon test. **J,** Immunofluorescence of SmoM2 cells with a magnified field showing the ciliary localization of ADORA2B (magenta) and cilia marker ARL13B (green). **K,** Representative images from H&E staining of ear skin from SmoM2 mice treated topically for 10 days with the indicated drugs or vehicle (control). **L,** Violin plot depicting the distribution of tumor burden of mice shown in **K**. $N = 15$ control, 12 BAY60-6583, 9 isoproterenol-treated mice, Welch *t* test. **M** and **N,** IF (**M**) and quantification (**N**) of the proliferation marker PCNA in mice shown in **K**. $N = 3$ mice per condition, ANOVA with *t* test. ns, nonsignificant; *, $P < 0.05$; **, $P < 0.01$; ***, $P < 0.001$; ****, $P < 0.0001$. **A,** Created in BioRender. Iglesias, R. (2025) https://BioRender.com/fr1j6fp.

inhibitory effect is also recapitulated in HEK293 cells, which lack cilia. These results highlight that ADORA2B can regulate Hedgehog through both ciliary and cytoplasmic effects. Notably, the SmoM2 mouse model represents SMO inhibitor–resistant BCC (23), indicating that targeting ADORA2B could be an alternative option for drug-resistant tumors.

The mouse models chosen for our study were based on characterizing the relationship between the Gαs pathway and canonical Hedgehog signaling. However, BCC mouse models have some limitations. BCC is one of the human cancers with the highest mutational burden (50, 54, 55), a fact that is not recapitulated in our single-oncogene BCC-like lesions. In addition, SmoM2 tumors are sometimes classified as basaloid follicular hamartomas (56, 57). Hamartomas are skin lesions with lower Hedgehog activation than BCC (56, 58). Despite this distinction, SmoM2 mice carry a mutation present in human BCC, recapitulate BCC development (59), and are extensively used as a model to study BCC. Another limitation of our study is that several of our experiments were performed in tail skin. However, it has been shown that tail scale and interscale domains are similar to human rete ridges and inter-ridges (29), making it a good parallel model to human skin.

Overall, our study provides a valuable resource to understand the developmental and pathologic roles of Gαs and Hedgehog signaling pathway cross-talk. The findings also reveal that oncogenic GPCR activation, such as SMO-driven signaling imbalances, can be counteracted by activating complementary pathways, restoring GPCR signaling equilibrium and normal physiologic processes essential for tissue homeostasis. Further research is needed to identify and expand the repertoire of signaling modulators capable of reestablishing normal cycles of stem cell proliferation and differentiation, ultimately restoring normal tissue function.

Data Availability

RNA-seq datasets generated for this study are publicly available in the Gene Expression Omnibus under accession codes GSE290008, GSE290004, and GSE290180. BCC mutation data were obtained from ref. 18 through cBioPortal (60). All other raw data are available from the corresponding author upon request.

Authors' Disclosures

No disclosures were reported.

Authors' Contributions

S. Krantz: Data curation, formal analysis, validation, investigation, visualization, methodology, writing–original draft, project administration, writing–review and editing. **B.A. Bell:** Data curation, formal analysis, validation, investigation, methodology. **K. Lund:** Data curation, formal analysis, funding acquisition, validation, investigation, visualization, writing–review and editing. **N. Salinas Parra:** Data curation, formal analysis, validation, investigation, visualization. **Y. Ng:** Data curation, formal analysis, validation, investigation, visualization, methodology. **N. De Oliveira Rosa:** Data curation, formal analysis, validation, investigation, visualization, methodology. **S. Mukhopadhyay:** Resources, data curation, writing–review and editing. **B. St. Croix:** Resources, data curation, writing–review and editing. **K.Y. Sarin:** Resources, data curation, formal analysis, investigation. **R. Weigert:** Resources, data curation, supervision, writing–review and editing. **F. Raimondi:** Resources, data curation, formal analysis, supervision, investigation, visualization, methodology, writing–review and editing. **R. Iglesias-Bartolome:** Conceptualization, resources, data curation, formal analysis, supervision, funding acquisition, validation, investigation, visualization, methodology, writing–original draft, project administration, writing–review and editing.

Acknowledgments

This research was supported by the Intramural Research Program of the National Institutes of Health (NIH) to R. Iglesias-Bartolome. The contributions of the NIH authors were made as part of their official duties as NIH federal employees, are in compliance with agency policy requirements, and are considered works of the U.S. government. However, the findings and conclusions presented in this article are those of the authors and do not necessarily reflect the views of the NIH or the U.S. Department of Health and Human Services. S. Mukhopadhyay was supported by grant R35GM144136. This work used the computational resources of the NIH High-Performance Computing Biowulf Cluster. Analysis and management of H&E images were supported by the NCI HALO Image Analysis Resource. The authors thank the members of the CCR Sequencing Facility at the Frederick National Laboratory for Cancer Research and the CCR Single Cell Analysis Facility for their help during sample preparation, sequencing, and data processing.

Note

Supplementary data for this article are available at Cancer Research Online (http://cancerres.aacrjournals.org/).

Received March 11, 2025; revised July 7, 2025; accepted December 18, 2025; posted first December 29, 2025.

References

1. Pedro MP, Lund K, Iglesias-Bartolome R. The landscape of GPCR signaling in the regulation of epidermal stem cell fate and skin homeostasis. Stem Cells 2020;38:1520–31.
2. Kong JH, Siebold C, Rohatgi R. Biochemical mechanisms of vertebrate hedgehog signaling. Development 2019;146:146.
3. Epstein EH. Basal cell carcinomas: attack of the hedgehog. Nat Rev Cancer 2008;8:743–54.
4. Rogers HW, Weinstock MA, Feldman SR, Coldiron BM. Incidence estimate of nonmelanoma skin cancer (keratinocyte carcinomas) in the U.S. Population, 2012. JAMA Dermatol 2015;151:1081–6.
5. Sekulic A, Von Hoff D. Hedgehog pathway inhibition. Cell 2016;164:831.
6. Peris K, Fargnoli MC, Kaufmann R, Arenberger P, Bastholt L, Seguin NB, et al. European consensus-based interdisciplinary guideline for diagnosis and treatment of basal cell carcinoma-update 2023. Eur J Cancer 2023;192:113254.
7. Iglesias-Bartolome R, Torres D, Marone R, Feng X, Martin D, Simaan M, et al. Inactivation of a Galpha(s)-PKA tumour suppressor pathway in skin stem cells initiates basal-cell carcinogenesis. Nat Cell Biol 2015;17:793–803.
8. Chen M, Gavrilova O, Zhao WQ, Nguyen A, Lorenzo J, Shen L, et al. Increased glucose tolerance and reduced adiposity in the absence of fasting hypoglycemia in mice with liver-specific Gs alpha deficiency. J Clin Invest 2005;115:3217–27.
9. Hwang SH, White KA, Somatilaka BN, Shelton JM, Richardson JA, Mukhopadhyay S. The G protein-coupled receptor Gpr161 regulates forelimb formation, limb patterning and skeletal morphogenesis in a primary cilium-dependent manner. Development 2018;145:145.
10. Cullen M, Elzarrad MK, Seaman S, Zudaire E, Stevens J, Yang MY, et al. GPR124, an orphan G protein-coupled receptor, is required for CNS-specific vascularization and establishment of the blood-brain barrier. Proc Natl Acad Sci U S A 2011;108:5759–64.
11. Yuan Y, Park J, Feng A, Awasthi P, Wang Z, Chen Q, et al. YAP1/TAZ-TEAD transcriptional networks maintain skin homeostasis by regulating cell proliferation and limiting KLF4 activity. Nat Commun 2020;11:1472.
12. Sasaki H, Hui C, Nakafuku M, Kondoh H. A binding site for Gli proteins is essential for HNF-3beta floor plate enhancer activity in transgenics and can respond to Shh in vitro. Development 1997;124:1313–22.
13. Yuan Y, Salinas PN, Chen Q, Iglesias-Bartolome R. Oncogenic hedgehog-smoothened signaling depends on YAP1–TAZ/TEAD transcription to restrain differentiation in basal cell carcinoma. J Invest Dermatol 2022;142:65–76.e7.
14. Cristofalo VJ, Allen RG, Pignolo RJ, Martin BG, Beck JC. Relationship between donor age and the replicative lifespan of human cells in culture: a reevaluation. Proc Natl Acad Sci U S A 1998;95:10614–9.
15. Uphoff CC, Drexler HG. Detecting mycoplasma contamination in cell cultures by polymerase chain reaction. Methods Mol Biol 2011;731:93–103.

16. Pedro MP, Salinas Parra N, Gutkind JS, Iglesias-Bartolome R. Activation of G-Protein coupled receptor-Galphai signaling increases keratinocyte proliferation and reduces differentiation, leading to epidermal hyperplasia. J Invest Dermatol 2020;140:1195–203.e3.
17. Korsunsky I, Millard N, Fan J, Slowikowski K, Zhang F, Wei K, et al. Fast, sensitive and accurate integration of single-cell data with harmony. Nat Methods 2019;16:1289–96.
18. Bonilla X, Parmentier L, King B, Bezrukov F, Kaya G, Zoete V, et al. Genomic analysis identifies new drivers and progression pathways in skin basal cell carcinoma. Nat Genet 2016;48:398–406.
19. McLaren W, Gil L, Hunt SE, Riat HS, Ritchie GR, Thormann A, et al. The ensembl variant effect predictor. Genome Biol 2016;17:122.
20. Melis N, Subramanian B, Chen D, Weigert R. Imaging neutrophil migration in the mouse skin to investigate subcellular membrane remodeling under physiological conditions. J Vis Exp 2022. DOI: https://doi.org/10.3791/63581.
21. Vasioukhin V, Degenstein L, Wise B, Fuchs E. The magical touch: genome targeting in epidermal stem cells induced by tamoxifen application to mouse skin. Proc Natl Acad Sci U S A 1999;96:8551–6.
22. Mao J, Ligon KL, Rakhlin EY, Thayer SP, Bronson RT, Rowitch D, et al. A novel somatic mouse model to survey tumorigenic potential applied to the Hedgehog pathway. Cancer Res 2006;66:10171–8.
23. Atwood SX, Sarin KY, Whitson RJ, Li JR, Kim G, Rezaee M, et al. Smoothened variants explain the majority of drug resistance in basal cell carcinoma. Cancer Cell 2015;27:342–53.
24. Belteki G, Haigh J, Kabacs N, Haigh K, Sison K, Costantini F, et al. Conditional and inducible transgene expression in mice through the combinatorial use of Cre-mediated recombination and tetracycline induction. Nucleic Acids Res 2005;33:e51.
25. Youssef KK, Lapouge G, Bouvree K, Rorive S, Brohee S, Appelstein O, et al. Adult interfollicular tumour-initiating cells are reprogrammed into an embryonic hair follicle progenitor-like fate during basal cell carcinoma initiation. Nat Cell Biol 2012;14:1282–94.
26. Depianto D, Kerns ML, Dlugosz AA, Coulombe PA. Keratin 17 promotes epithelial proliferation and tumor growth by polarizing the immune response in skin. Nat Genet 2010;42:910–4.
27. Joost S, Zeisel A, Jacob T, Sun X, La Manno G, Lonnerberg P, et al. Single-cell transcriptomics reveals that differentiation and spatial signatures shape epidermal and hair follicle heterogeneity. Cell Syst 2016;3:221–37.e9.
28. Quigley DA, Kandyba E, Huang P, Halliwill KD, Sjolund J, Pelorosso F, et al. Gene expression architecture of mouse dorsal and tail skin reveals functional differences in inflammation and cancer. Cell Rep 2016;16:1153–65.
29. Ghuwalewala S, Lee SA, Jiang K, Baidya J, Chovatiya G, Kaur P, et al. Binary organization of epidermal basal domains highlights robustness to environmental exposure. EMBO J 2022;41:e110488.
30. Nguyen MB, Flora P, Branch MC, Weber M, Zheng XY, Sivan U, et al. Tenascin-C expressing touch dome keratinocytes exhibit characteristics of all epidermal lineages. Sci Adv 2024;10:eadi5791.
31. Yang Y, Gomez N, Infarinato N, Adam RC, Sribour M, Baek I, et al. The pioneer factor SOX9 competes for epigenetic factors to switch stem cell fates. Nat Cell Biol 2023;25:1185–95.
32. Powell AE, Wang Y, Li Y, Poulin EJ, Means AL, Washington MK, et al. The pan-ErbB negative regulator Lrig1 is an intestinal stem cell marker that functions as a tumor suppressor. Cell 2012;149:146–58.
33. Barker N, van Es JH, Kuipers J, Kujala P, van den Born M, Cozijnsen M, et al. Identification of stem cells in small intestine and colon by marker gene Lgr5. Nature 2007;449:1003–7.
34. Weigert R, Sramkova M, Parente L, Amornphimoltham P, Masedunskas A. Intravital microscopy: a novel tool to study cell biology in living animals. Histochem Cell Biol 2010;133:481–91.
35. Niewiadomski P, Kong JH, Ahrends R, Ma Y, Humke EW, Khan S, et al. Gli protein activity is controlled by multisite phosphorylation in vertebrate Hedgehog signaling. Cell Rep 2014;6:168–81.
36. Mukhopadhyay S, Wen X, Ratti N, Loktev A, Rangell L, Scales SJ, et al. The ciliary G-protein-coupled receptor Gpr161 negatively regulates the Sonic hedgehog pathway via cAMP signaling. Cell 2013;152:210–23.
37. Shimada IS, Hwang SH, Somatilaka BN, Wang X, Skowron P, Kim J, et al. Basal suppression of the sonic Hedgehog pathway by the G-Protein-Coupled receptor Gpr161 restricts medulloblastoma pathogenesis. Cell Rep 2018;22:1169–84.
38. Bai CB, Auerbach W, Lee JS, Stephen D, Joyner AL. Gli2, but not Gli1, is required for initial Shh signaling and ectopic activation of the Shh pathway. Development 2002;129:4753–61.
39. He X, Zhang L, Chen Y, Remke M, Shih D, Lu F, et al. The G protein alpha subunit Galphas is a tumor suppressor in Sonic hedgehog-driven medulloblastoma. Nat Med 2014;20:1035–42.
40. Eckle T, Krahn T, Grenz A, Kohler D, Mittelbronn M, Ledent C, et al. Cardioprotection by ecto-5'-nucleotidase (CD73) and A2B adenosine receptors. Circulation 2007;115:1581–90.
41. Happ JT, Arveseth CD, Bruystens J, Bertinetti D, Nelson IB, Olivieri C, et al. A PKA inhibitor motif within SMOOTHENED controls Hedgehog signal transduction. Nat Struct Mol Biol 2022;29:990–9.
42. Pusapati GV, Kong JH, Patel BB, Gouti M, Sagner A, Sircar R, et al. G protein-coupled receptors control the sensitivity of cells to the morphogen Sonic Hedgehog. Sci Signaling 2018;11:eaao5749.
43. Somatilaka BN, Hwang SH, Palicharla VR, White KA, Badgandi H, Shelton JM, et al. Ankmy2 prevents smoothened-independent hyperactivation of the hedgehog pathway via Cilia-regulated adenylyl cyclase signaling. Dev Cell 2020;54:710–26.e8.
44. Youssef KK, Van Keymeulen A, Lapouge G, Beck B, Michaux C, Achouri Y, et al. Identification of the cell lineage at the origin of basal cell carcinoma. Nat Cell Biol 2010;12:299–305.
45. Peterson SC, Eberl M, Vagnozzi AN, Belkadi A, Veniaminova NA, Verhaegen ME, et al. Basal cell carcinoma preferentially arises from stem cells within hair follicle and mechanosensory niches. Cell Stem Cell 2015;16:400–12.
46. Grachtchouk M, Pero J, Yang SH, Ermilov AN, Michael LE, Wang A, et al. Basal cell carcinomas in mice arise from hair follicle stem cells and multiple epithelial progenitor populations. J Clin Invest 2011;121:1768–81.
47. Wang GY, Wang J, Mancianti ML, Epstein EH Jr. Basal cell carcinomas arise from hair follicle stem cells in Ptch1(+/-) mice. Cancer Cell 2011;19:114–24.
48. Veniaminova NA, Vagnozzi AN, Kopinke D, Do TT, Murtaugh LC, Maillard I, et al. Keratin 79 identifies a novel population of migratory epithelial cells that initiates hair canal morphogenesis and regeneration. Development 2013;140:4870–80.
49. Choquet H, Ashrafzadeh S, Kim Y, Asgari MM, Jorgenson E. Genetic and environmental factors underlying keratinocyte carcinoma risk. JCI Insight 2020;5:e134783.
50. Kilgour JM, Jia JL, Sarin KY. Review of the molecular genetics of basal cell carcinoma; inherited susceptibility, somatic mutations, and targeted therapeutics. Cancers (Basel) 2021;13:3870.
51. Chiang A, Solis DC, Rogers H, Sohn GK, Cho HG, Saldanha G, et al. Prevalence and risk factors for high-frequency basal cell carcinoma in the United States. J Am Acad Dermatol 2021;84:1493–5.
52. Liu Y, Banka S, Huang Y, Hardman-Smart J, Pye D, Torrelo A, et al. Germline intergenic duplications at Xq26.1 underlie Bazex-Dupre-Christol basal cell carcinoma susceptibility syndrome. Br J Dermatol 2022;187:948–61.
53. Eccles RL, Czajkowski MT, Barth C, Muller PM, McShane E, Grunwald S, et al. Bimodal antagonism of PKA signalling by ARHGAP36. Nat Commun 2016;7:12963.
54. Chalmers ZR, Connelly CF, Fabrizio D, Gay L, Ali SM, Ennis R, et al. Analysis of 100,000 human cancer genomes reveals the landscape of tumor mutational burden. Genome Med 2017;9:34.
55. Jayaraman SS, Rayhan DJ, Hazany S, Kolodney MS. Mutational landscape of basal cell carcinomas by whole-exome sequencing. J Invest Dermatol 2014;134:213–20.
56. Grachtchouk V, Grachtchouk M, Lowe L, Johnson T, Wei L, Wang A, et al. The magnitude of hedgehog signaling activity defines skin tumor phenotype. EMBO J 2003;22:2741–51.
57. Yang SH, Andl T, Grachtchouk V, Wang A, Liu J, Syu LJ, et al. Pathological responses to oncogenic Hedgehog signaling in skin are dependent on canonical Wnt/beta3-catenin signaling. Nat Genet 2008;40:1130–5.
58. Tjarks BJ, Gardner JM, Riddle ND. Hamartomas of skin and soft tissue. Semin Diagn Pathol 2019;36:48–61.
59. Xie J, Murone M, Luoh SM, Ryan A, Gu Q, Zhang C, et al. Activating smoothened mutations in sporadic basal-cell carcinoma. Nature 1998;391:90–2.
60. Cerami E, Gao J, Dogrusoz U, Gross BE, Sumer SO, Aksoy BA, et al. The cBio cancer genomics portal: an open platform for exploring multidimensional cancer genomics data. Cancer Discov 2012;2:401–4.